

**Dongming Gan**<sup>1</sup>

Robotics Institute,  
Khalifa University of Science,  
Technology and Research,  
Abu Dhabi 127788, UAE  
e-mail: dongming.gan@kustar.ac.ae

**Jian S. Dai**

School of Natural and Mathematical Sciences,  
King's College London,  
University of London,  
London WC2R2LS, UK

**Jorge Dias**

Robotics Institute,  
Khalifa University of Science,  
Technology and Research,  
Abu Dhabi 127788, UAE;  
Faculty of Science and Technology,  
University of Coimbra,  
Coimbra 3000-315, Portugal

**Lakmal Seneviratne**

Robotics Institute,  
Khalifa University of Science,  
Technology and Research,  
Abu Dhabi 127788, UAE;  
School of Natural and Mathematical Sciences,  
King's College London,  
University of London,  
London WC2R2LS, UK

# Unified Kinematics and Singularity Analysis of a Metamorphic Parallel Mechanism With Bifurcated Motion

*This paper introduces a new metamorphic parallel mechanism consisting of four reconfigurable rTPS limbs. Based on the reconfigurability of the reconfigurable Hooke (rT) joint, the rTPS limb has two phases while in one phase the limb has no constraint to the platform, in the other it constrains the spherical joint center to lie on a plane. This results in the mechanism to have ability of reconfiguration between different topologies with variable mobility. Geometric constraint equations of the platform rotation matrix and translation vector are set up based on the point-plane constraint, which reveals the bifurcated motion property in the topology with mobility 2 and the geometric condition with mobility change in altering to other mechanism topologies. Following this, a unified kinematics limb modeling is proposed considering the difference between the two phases of the reconfigurable rTPS limb. This is further applied for the mechanism modeling and both the inverse and forward kinematics is analytically solved by combining phases of the four limbs covering all the mechanism topologies. Based on these, a unified singularity modeling is proposed by defining the geometric constraint forces and actuation forces in the Jacobian matrix with their change in the variable topologies in terms of constraint screws. Analysis of workspace with singularity distribution is carried out using this model and corresponding singularity loci are obtained with special singular configurations illustrated. [DOI: 10.1115/1.4024292]*

*Keywords:* parallel mechanism, reconfiguration, unified kinematics, workspace, singularity

## 1 Introduction

Inheriting the advantages of traditional parallel mechanisms in terms of high load-carrying capacity, good positioning accuracy and low inertia [1], metamorphic parallel mechanisms (MPMs) [2] also possess adaptability and reconfigurability to change permanent finite mobility based on the topological structure change. Metamorphic parallel mechanisms can replace the traditional ones in real applications with benefits of configuration change for special workspace requirements, operation mobility change or energy saving in the industry and other areas. The 4rTPS metamorphic parallel mechanism introduced in this paper has ability of mobility change from 2 to 6, bifurcated rotation about two orthogonal axes and symmetrical mechanism structure. These properties make this mechanism suitable for some applications in industry machining, product assembly, motion simulation, and human joint rehabilitation with requirements of mobility change and separate rotation motions in two orthogonal directions, like training on the two rotations (inversion/eversion and flexion/extension) of ankle rehabilitation, machining, simulation, and assembly in two perpendicular planes.

Proposed from the study of decorative carton folds and reconfigurable packaging [3], metamorphic mechanisms have attracted much interest in the mechanism research due to their novel property of reconfiguration and mobility change. These include kinematotropic linkages with variable position parameters [4],

orthoplanar metamorphic mechanisms [5], metamorphic underwater vehicle [6], metamorphic ways of changing the topological structures of a mechanism [7], topology description of various mobility configurations of metamorphic mechanisms using matrix operations [8], variable topologies of kinematic joints and their topological representation [9,10], kinematotropic parallel mechanisms with variable motions [11], reconfigurable parallel robot [12], and a family of parallel mechanisms that have multiple operation modes [13]. Recent work is on a metamorphic multifingered hand with an articulated palm [14], methodology for synthesis and configuration design of metamorphic mechanisms based on biological modeling and genetic evolution [15], a metamorphic parallel mechanism with ability of performing phase change and orientation switch [16].

Based on a newly invented reconfigurable Hooke (rT) joint [2], various metamorphic parallel mechanisms [2,17] have been presented with a general construction method introduced using screw theory [18]. This leads to the work of this paper of a new metamorphic parallel mechanism consisting of reconfigurable rTPS limbs. In the one phase, the rTPS limb has mobility 6 while it supplies one constraint force in the other phase which can be geometrically interpreted as constraining a point of the platform to lie on a plane. This point-plane constraint was studied by Wampler [19] in workspace analysis of a 3-degrees of freedom (DOF) tripod mechanism and Selig [20] in instantaneous kinematics of parallel mechanisms using dual quaternions. The point-plane constraint was also called planar-spherical bond by Karouia and Hervé [21] with a serial arrangement of a planar kinematic bond and a spherical bond. Various planar-spherical serial chains were illustrated with mobility analysis based on Lie group theory and were used for parallel mechanism construction [22,23].

<sup>1</sup>Corresponding author.

Contributed by the Mechanisms and Robotics Committee of ASME for publication in the JOURNAL OF MECHANISMS AND ROBOTICS. Manuscript received July 18, 2012; final manuscript received March 28, 2013; published online June 24, 2013. Assoc. Editor: Qiaode Jeffrey Ge.

The metamorphic parallel mechanism investigated in this paper has an interesting property of bifurcated rotation motion in the topology with mobility 2. Bifurcated motion [24,25] is the phenomenon that the mechanism motion has two branches when it passes through the constraint singularity [26,27], resulting in different mobility and scope of motion. Similar to this topology with mobility 2, [28] used the 4RPS parallel mechanism in the exoskeleton of the shoulder part with different shapes between the platform and the base [29]. Proposed a  $4R_b$ RPS parallel mechanism (where  $R_b$  denotes a lockable revolute joint at any time during operation through a brake) with limbs that can change between equivalent universal joint-prismatic joint-spherical joint (UPS) and revolute joint-prismatic joint-spherical joint (RPS). Motion planning was investigated considering the transition among different configurations by locking different  $R_b$  joints on the base. With different focus, bifurcated motion was not revealed in the previous research.

Following the structure synthesis and mobility analysis, the next important topics are kinematics and singularity analysis which are the base for further dynamic investigation and mechanism applications. While inverse kinematics is easy, forward kinematics of a parallel mechanism is considered as a very complex problem due to the fact that it normally leads to high order polynomial equations with multisolutions [30,31]. Analytically solving the forward kinematics by obtaining the univariant equation with one unknown is the idea result as it gives straightforward solutions and the inter-relations for variable geometry parameters. Since a metamorphic parallel mechanism has several topologies with different mobility, each of them is a traditional parallel mechanism. Thus, to get a unified kinematics modeling is a big challenge by covering all the mechanism topologies and solving each one analytically. In this paper, based on the difference between the two phases of the reconfigurable rTPS limb, a unified kinematics limb modeling is proposed. This is further applied for the mechanism modeling, based on which forward kinematics analysis with univariant equations in one unknown are obtained by combining phases of the four limbs corresponding to various topologies. The unified kinematics modeling method can be used for other metamorphic parallel mechanisms consisting of rTPS limbs.

Following the kinematics analysis, a unified singularity modeling to cover all the reconfigurable topologies is presented based on constraint screws. In parallel mechanism research, singularity analysis [32,33] is an important topic as singularities will make the mechanism dysfunctional and uncontrollable which should be avoided and considered before parameter design for real applications. Many methods have been proposed for singularity analysis, including Jacobian-determinant-based numerical methods [34], Jacobian-rank-based analytical models [32,35], screw theory [36,37], line geometry, and Grassmann-Cayley algebra [38,39]. Considering the variable topologies of the metamorphic parallel mechanism in this paper, screw theory shows a good way to formulate a unified Jacobian matrix to include both geometric constraints and actuation constraints with change between them in the reconfiguration while the size is kept 6 by 6. The method introduced in this paper can be extended to other parallel mechanisms with variable topologies and mobility.

The paper is arranged in the following structure. Section 2 introduced the reconfigurable rTPS limb with two phases and their geometric modeling. Starting from a topology with bifurcated motion in Sec. 3, geometric constraints are set up for the mobility analysis, and then various topology reconfigurations are illustrated and analyzed in Sec. 4. Based on this, Sec. 5 proposes a unified limb kinematics modeling and solves both inverse and forward kinematics analytically for all the topologies. The unified Jacobian matrix is presented in Sec. 6 with constraint screw changes in workspace analysis with singularity distribution in variable topologies. Conclusions are summed in Sec. 7.

## 2 Two Phases of the Reconfigurable rTPS Limb

The reconfigurable rTPS limb consists of a reconfigurable Hooke (rT) joint, a prismatic joint, and a spherical joint. The

reconfigurability of this limb stems from the configuration change of the rT joint which has two rotational DOFs about two perpendicularly intersecting rotational axes (radial axis and bracket axis) as in Fig. 1. A grooved ring is used to house the radial axis and make it have the ability of altering its direction by rotating and fixing freely along the groove. This allows the radial rotation axis change with respect to the limb, resulting in two typical phases of the rTPS limb as in Fig. 1. While in Fig. 1(a), the radial axis is perpendicular to the limb (prismatic joint) which is denoted as  $(rT)_1PS$ , it is collinear with the limb (prismatic joint) passing through the spherical joint center in Fig. 1(b) and the limb phase is symbolized as  $(rT)_2PS$ .

Set an arbitrary coordinate system  $oxyz$  as in Fig. 1(a). Let points  $A$  and  $B$  denote the spherical joint center and the rT joint center, respectively,  $\mathbf{a}$  and  $\mathbf{b}$  denote the vectors of points  $A$  and  $B$  in the  $oxyz$  coordinate system. Let the distance between  $A$  and  $B$  is  $h$ , then the geometric constraint of the  $(rT)_1PS$  limb is given as

$$\begin{cases} (\mathbf{a} - \mathbf{b})^2 = h^2 \\ (\mathbf{a} - \mathbf{b}) \cdot \mathbf{n} = h \cos(\phi_1 + \pi/2) \\ \frac{((\mathbf{a} - \mathbf{b}) - ((\mathbf{a} - \mathbf{b}) \cdot \mathbf{n})\mathbf{n}) \cdot \mathbf{n}_0}{\|(\mathbf{a} - \mathbf{b}) - ((\mathbf{a} - \mathbf{b}) \cdot \mathbf{n})\mathbf{n}\|} = \cos\phi_2 \end{cases} \quad (1)$$

which shows that position of the spherical joint center  $A$  is determined by stroke ( $h$ ) of the prismatic joint and rotational angles (radial axis angle  $\phi_1$  and bracket axis angle  $\phi_2$ ) of the rT joint as in Fig. 1, where  $\phi_1$  is between the limb and its projection on plane  $\Sigma$  passing through  $AB$  and perpendicular to the bracket axis ( $\mathbf{n}$ ) of the rT joint,  $\mathbf{n}_0$  is a reference line passing through rT joint center  $B$  and perpendicular to  $\mathbf{n}$ . This describes the forward kinematics of the limb. Inversely, stroke ( $h$ ) and rotational angles ( $\phi_1$  and  $\phi_2$ ) can be calculated directly from Eq. (1) when the spherical joint center  $A$  is known.

For the  $(rT)_2PS$  limb as in Fig. 1(b), radial axis of the rT joint is collinear with the prismatic joint passing through the spherical joint center  $A$ . Thus, the spherical joint center  $A$  cannot move out of the plane  $\Sigma$ . Geometric constraint of the  $(rT)_2PS$  limb is given as

$$\begin{cases} (\mathbf{a} - \mathbf{b})^2 = h^2 \\ (\mathbf{a} - \mathbf{b}) \cdot \mathbf{n} = \mathbf{a} \cdot \mathbf{n} - d = 0 \\ (\mathbf{a} - \mathbf{b}) \cdot \mathbf{n}_0 = h \cos\phi_2 \end{cases} \quad (2)$$

which shows that position of the spherical joint center  $A$  is determined by stroke ( $h$ ) of the prismatic joint and bracket axis angle ( $\phi_2$ ) of the rT joint.  $d$  is the distance from the coordinate system center  $o$  to plane  $\Sigma$ . Equation (2) describes both forward and inverse kinematics of the  $(rT)_2PS$  limb.

From Eqs. (1) and (2) it can be seen that the  $(rT)_2PS$  limb has one degree of freedom less than the  $(rT)_1PS$  limb as it has one more constraint. In fact, the  $(rT)_1PS$  limb has six DOFs and the  $(rT)_2PS$  limb has five [2]. When constructing parallel mechanisms

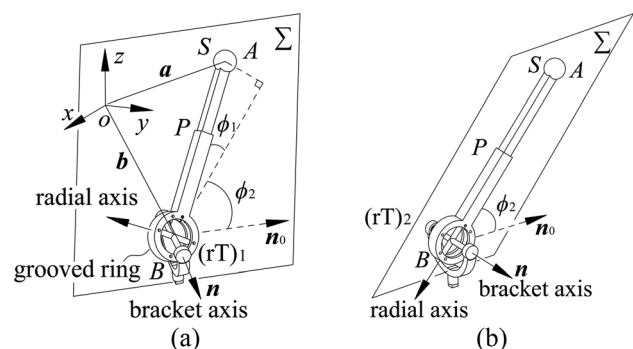


Fig. 1 Two phases of the rTPS limb (a)  $(rT)_1PS$  and (b)  $(rT)_2PS$

with the rTPS limbs, the mechanisms will have ability of mobility change by altering the rTPS limbs into these two phases.

### 3 The 4(rT)<sub>2</sub>PS MPM With Bifurcated Motion

The 4(rT)<sub>2</sub>PS metamorphic parallel mechanism consisting of four (rT)<sub>2</sub>PS limbs is shown in Fig. 2, in which the four limbs are arranged symmetrically on a circle with radius  $r_a$  on the platform and a circle with radius  $r_b$  on the base. Let  $A_i$  be the center point of the spherical joint and  $B_i$  be the rT joint center in limb  $i$  as Fig. 2. Locate a fixed coordinate system  $Oxyz$  at the geometric center  $O$  of the square  $B_1B_2B_3B_4$  with  $x$ -axis passing through  $B_1$  and  $y$ -axis passing through  $B_2$ . Similarly, attach a platform coordinate system  $Guvw$  at the geometric center  $G$  of square  $A_1A_2A_3A_4$  with  $u$ -axis passing through  $A_1$  and  $v$ -axis passing through  $A_2$ . Based on the geometric constraint in Eq. (2), the spherical joint centers  $A_i$  are constrained in their own planes

$$\begin{cases} \mathbf{a}_i \cdot (0,1,0)^T = (\mathbf{R}\mathbf{a}'_i + \mathbf{p}) \cdot (0,1,0)^T = 0 & (i = 1,3) \\ \mathbf{a}_j \cdot (1,0,0)^T = (\mathbf{R}\mathbf{a}'_j + \mathbf{p}) \cdot (1,0,0)^T = 0 & (j = 2,4) \end{cases} \quad (3)$$

where  $\mathbf{a}'_i$  is the vector of  $A_i$  expressed in the platform coordinate system  $Guvw$  and can be given as  $\mathbf{a}'_1 = -\mathbf{a}'_3 = r_a(1,0,0)^T$ ,  $\mathbf{a}'_2 = -\mathbf{a}'_4 = r_a(0,1,0)^T$ ,  $\mathbf{R} = (\mathbf{u}, \mathbf{v}, \mathbf{w})$ , and  $\mathbf{p} = (p_x, p_y, p_z)^T$  are the transformation matrix and the translation vector of platform coordinate system  $Guvw$  with respect to the fixed coordinate system  $Oxyz$ ,  $\mathbf{u}, \mathbf{v}, \mathbf{w}$  are unit vectors of the axes of platform coordinate system  $Guvw$  expressed in the fixed coordinate system  $Oxyz$  with  $\mathbf{u} = (u_x, u_y, u_z)^T$ ,  $\mathbf{v} = (v_x, v_y, v_z)^T$ , and  $\mathbf{w} = (w_x, w_y, w_z)^T$ .

From Eq. (3) and the above assumption, there is

$$\begin{cases} (a_1 - a_3) = \mathbf{R}(\mathbf{a}'_1 - \mathbf{a}'_3) \cdot (0,1,0)^T = r_a \mathbf{u} \cdot (0,1,0)^T = r_a u_y = 0 \\ (a_2 - a_4) = \mathbf{R}(\mathbf{a}'_2 - \mathbf{a}'_4) \cdot (1,0,0)^T = r_a \mathbf{v} \cdot (1,0,0)^T = r_a v_x = 0 \end{cases} \quad (4)$$

Thus, there is  $v_x = 0$  and  $u_y = 0$ , substituting these into the orthogonal property of matrix  $\mathbf{R}$  leads to the following:

$$u_x v_x + u_y v_y + u_z v_z = u_z v_z = 0 \quad (5)$$

The above equation presents two possible rotations but cannot be simultaneously executed. This leads to two bifurcated rotations and a home position based on three motion possibilities. They are home position when  $u_z = v_z = 0$  with rotation matrix  $\mathbf{R}$  becoming the identity matrix  $\mathbf{I}$ , branch 1 motion as  $u_z = 0, v_z \neq 0$  with  $\mathbf{R}$  as a pure rotation about  $x$ -axis and branch 2 motion as  $u_z \neq 0, v_z = 0$  with  $\mathbf{R}$  as a pure rotation about  $y$ -axis. This indicates whenever if the platform tilts to one direction from the constraint singularity, it falls into that directional rotation. Vice versa, when the platform tilts to another direction, it falls into another directional rotation. These two motions cannot be executed simultaneously.

Expanding Eq. (3) when  $i = 1$  and  $j = 2$ , there is

$$\begin{cases} (\mathbf{R}\mathbf{a}'_1 + \mathbf{p}) \cdot (0,1,0)^T = r_a u_y + p_y = p_y = 0 \\ (\mathbf{R}\mathbf{a}'_2 + \mathbf{p}) \cdot (1,0,0)^T = r_a v_x + p_x = p_x = 0 \end{cases} \quad (6)$$

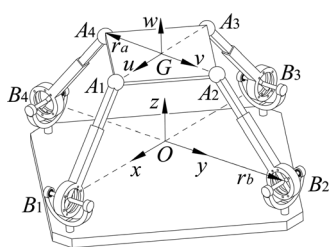


Fig. 2 The 4(rT)<sub>2</sub>PS MPM with bifurcated motion

which determines the property of the translation vector  $\mathbf{p}$  with elements on  $x$ -axis and  $y$ -axis being zeros.

From the above analysis, it can be concluded that the four geometric constraints in Eq. (3) lead to two rotational constraints in Eq. (4) and two translational constraints in Eq. (6). Thus, the mechanism has one translation along  $z$ -axis and one rotation, a pure rotation either about  $x$ -axis or  $y$ -axis, bifurcated based on Eq. (5).

### 4 Topology Change Based Reconfiguration of the 4(rT)<sub>2</sub>PS MPM

When altering the limb phases from (rT)<sub>2</sub>PS to (rT)<sub>1</sub>PS, the 4(rT)<sub>2</sub>PS parallel mechanism will change to different topologies with variable mobility. First, changing the phase of limb 1, the mechanism becomes the topology 3(rT)<sub>2</sub>PS-1(rT)<sub>1</sub>PS as in Fig. 3(a). Based on the geometric relation in Eq. (1), there will be one geometric constraint less in the mechanism in Eq. (3) by reducing  $i = 1$  for limb 1. Then, the relation can be given as

$$\begin{cases} r_a u_y + p_y = 0 \\ r_a v_x + p_x = p_x = 0 \\ v_x = 0 \end{cases} \quad (7)$$

which shows that there is one constraint for the rotation with  $v_x = 0$  and two constraints for the translation with  $p_x = 0$  and  $p_y$  depending on the rotation. Thus, the 3(rT)<sub>2</sub>PS-1(rT)<sub>1</sub>PS parallel mechanism has mobility three with two rotations and one translation.

When further changing the phase of limb 2, the mechanism becomes the topology 2(rT)<sub>2</sub>PS-2(rT)<sub>1</sub>PS as in Fig. 3(b). Hence, one more constraint vanishes in Eq. (3) and the geometric constraints become

$$\begin{cases} r_a u_y + p_y = 0 \\ r_a v_x + p_x = 0 \end{cases} \quad (8)$$

which presents that the translation elements  $p_x$  and  $p_y$  depend on the platform rotation and there is no constraint on the rotation matrix. Thus, the 2(rT)<sub>2</sub>PS-2(rT)<sub>1</sub>PS parallel mechanism has mobility four with three rotations and one independent translation along  $z$ -axis.

Following the above, a new topology 1(rT)<sub>2</sub>PS-3(rT)<sub>1</sub>PS will be obtained by changing the phase of limb 3 as in Fig. 3(c). In this case, only the second constraint in Eq. (8) is left, indicating that translation elements  $p_x$  can be determined by the platform

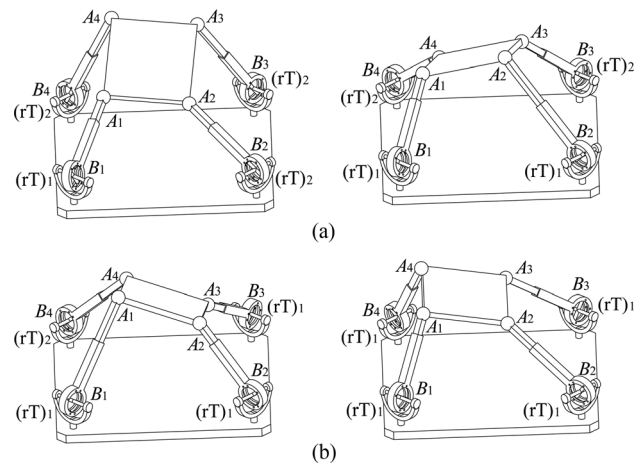


Fig. 3 Variable topologies of the 4(rT)PS MPM (a) 3(rT)<sub>2</sub>PS-1(rT)<sub>1</sub>PS (1T2R), (b) 2(rT)<sub>2</sub>PS-2(rT)<sub>1</sub>PS (2T2R), (c) 1(rT)<sub>2</sub>PS-3(rT)<sub>1</sub>PS (2T3R), and (d) 4(rT)<sub>1</sub>PS (3T3R)

rotation. Thus, the new mechanism has five degrees of freedom with one translation along  $x$ -axis constrained.

Finally, after further changing the forth limb into phase  $(rT)_1PS$ , the mechanism becomes the topology  $4(rT)_1PS$  as in Fig. 3(d) with full mobility 6 as there is no geometric constraints for the platform by the limbs.

From this, it can be seen that the limb phases determine the topology and mobility of the mechanism. It is worth noticing that when changing the limb phases in different orders, the mechanism can have different topologies with those in Fig. 3. For example, in the reconfiguration from topology  $3(rT)_2PS-1(rT)_1PS$  in Fig. 3(a) to  $2(rT)_2PS-2(rT)_1PS$  in Fig. 3(b), when altering the phase of limb 2 instead of limb 1, the mechanism becomes a new topology  $2(rT)_2PS-2(rT)_{13}PS$  with mobility four of two translations and two rotations. Here,  $rT_{13}$  is used to indicate that the  $(rT)_1PS$  phases are from limb 1 and limb 3. Based on this, all the topologies with variable mobility are concluded in Table 1, in which  $1R_{x/y}$  represents the bifurcated rotation about  $x$ -axis or  $y$ -axis,  $2R_{xy}$  means two rotations about  $x$ -axis and  $y$ -axis,  $1T_z$ ,  $2T_{xz}$ , and  $2T_{yz}$  indicate 1 or 2 translations along the corresponding axes in the subscripts. In Table 1, any two mobility types can be changed into each other directly by changing corresponding limb phases. For example, when changing the phases of limb 2 and limb 4 from  $(rT)_2PS$  to  $(rT)_1PS$  in  $4(rT)_2PS$ , the topology can be directly change into  $2(rT)_2PS-2(rT)_{24}PS$  with mobility  $2T_{yz}2R_{xy}$ . When further altering the other two limb phases to  $(rT)_1PS$ , the mechanism becomes directly to  $4(rT)_1PS$  with full mobility  $3T3R$ . The inverse phase change also works.

## 5. Unified Kinematics Modeling and Displacement Analysis

In the  $rTPS$  limb, there are three single DOF joints that can be selected as actuated joints, including the two rotational joints of the  $rT$  joint and the prismatic joint. The actuation scheme requires that the selected actuations can determine the platform position and orientation with finite forward kinematics solutions. Based on these, it can be found that any actuation selection from the three single DOF joints in the four limbs of the  $4rTPS$  metamorphic parallel mechanism with corresponding number of mechanism mobility can satisfy the actuation scheme requirement except the case of  $4(rT)_2PS$  with bifurcation which requires that the inputs should be from two adjacent limbs. Considering the simplicity of kinematics analysis and that prismatic joints give better force transmission than revolute joints, the four prismatic joints in the mechanism and the two radial rotational joints in limb 1 and limb 2 are selected as the actuated joints corresponding to variable topologies. For mobility  $n$  ( $2 \leq n \leq 4$ ),  $n$  prismatic joints will be active, while  $4-n$  prismatic joints and the two radial joints are passive. When the mechanism is in mobility 5, the four prismatic joints with one of the two radial joints will be active. All the six joints are active when coming to mobility 6.

**5.1 Unified Limb Kinematics Modeling.** For limb 1 and limb 2, when they are in the phase  $(rT)_2PS$ , their prismatic joints are chosen as the actuations. When they are altered into phase

**Table 1 Variable topologies and mobility of the 4rTPS**

Mobility	DOFs	Topologies
2	$1T_z1R_{x/y}$	$4(rT)_2PS$
3	$1T_z2R_{xy}$	$3(rT)_2PS-1(rT)_iPS$ ( $i = 1, 2, 3, 4$ )
4	$2T_{xz}2R_{xy}$	$2(rT)_2PS-2(rT)_{13}PS$
	$2T_{yz}2R_{xy}$	$2(rT)_2PS-2(rT)_{24}PS$
	$1T_z3R$	$2(rT)_2PS-2(rT)_{ij}PS$ ( $i = 1, 3, j = 2, 4$ )
5	$2T_{xz}3R$	$1(rT)_i2PS-3(rT)_jPS$ ( $i = 2, 4$ )
	$2T_{yz}3R$	$1(rT)_i2PS-3(rT)_jPS$ ( $i = 1, 3$ )
6	$3T3R$	$4(rT)_1PS$

$(rT)_1PS$ , by further selecting the radial axis rotation as the input, a unified kinematics model can be obtained. This is due to the difference between the two phases of the  $rTPS$  limb as in Fig. 1. It can be taken as that the  $(rT)_1PS$  limb has variable radial axis angle  $\phi_1$ , while the  $(rT)_2PS$  limb has a fixed angle  $\phi_1 = 0$ . Geometrically, spherical joint center  $A$  is constrained on plane  $\Sigma\phi_1$  passing through the spherical joint center and perpendicular to the bracket axis for a giving angle  $\phi_1$  in the  $(rT)_1PS$  limb and it is constrained on plane  $\Sigma 0$  passing through the  $rT$  joint center and perpendicular to the bracket axis in the  $(rT)_2PS$  limb as in Fig. 4.

Based on the above analysis and the coordinate systems of the  $3rTPS$  metamorphic parallel mechanism in Figs. 4 and 2, the geometric constraint of the mechanism relating to limb 1 and limb 2 can be expressed in the fixed coordinate system  $Oxyz$  by covering their two phases as

$$\begin{cases} \mathbf{a}_1 = \mathbf{b}_1 + \mathbf{R}(z, \pi/2)l_1(-\sin\phi_{11}, \cos\phi_{11}\cos\phi_{12}, \cos\phi_{11}\sin\phi_{12}) \\ \mathbf{a}_2 = \mathbf{b}_2 + \mathbf{R}(z, \pi)l_2(-\sin\phi_{21}, \cos\phi_{21}\cos\phi_{22}, \cos\phi_{21}\sin\phi_{22}) \end{cases} \quad (9)$$

where  $l_i$  and  $\phi_{i1}$  are the length and radial rotation angle of limb  $i$  separately,  $\phi_{i1} = 0$  for  $(rT)_2PS$  and it is an unknown for  $(rT)_1PS$ .  $\mathbf{R}(k, g)$  represents a rotation about axis  $k$  with angle  $g$  and is used to translate the vector of the spherical joint center in the limb coordinate systems to the global coordinate system in Fig. 2.

For limb 3 and limb 4, when they are in the phase  $(rT)_2PS$ , no actuation is selected from them. When they are altered into phase  $(rT)_1PS$ , their prismatic joints will be the actuated joints. Thus, the kinematics modeling is

$$\begin{cases} (\mathbf{a}_3 - \mathbf{b}_3) \cdot (\mathbf{a}_3 - \mathbf{b}_3) = l_3^2; & (\mathbf{a}_4 - \mathbf{b}_4) \cdot (\mathbf{a}_4 - \mathbf{b}_4) = l_4^2 & (rT)_1PS \\ \mathbf{a}_3 \cdot (0, 1, 0)^T = 0; & \mathbf{a}_4 \cdot (1, 0, 0)^T = 0 & (rT)_2PS \end{cases} \quad (10)$$

where  $\mathbf{a}_3 = (x_3, y_3, z_3)^T$ ,  $\mathbf{a}_4 = \mathbf{a}_1 + \mathbf{a}_3 - \mathbf{a}_2$ .

By combining the above limb models in different phases, all the kinematics modeling of the reconfigurable topologies of the  $4rTPS$  metamorphic parallel mechanism can be obtained. They can be solved inversely and forwardly in the following way.

## 5.2 Inverse and Forward Kinematics Analysis

**5.2.1 Inverse Kinematics Analysis** The inverse displacement analysis of the  $4rTPS$  metamorphic parallel mechanism is to obtain the actuation parameters (limb length  $l_i$ , radial-axis rotation angle  $\phi_{i1}$ ) based on the given platform position and orientation.

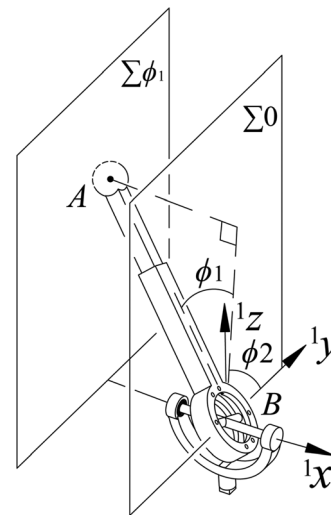


**Fig. 4 Unified limb modeling**

Based on Eqs. (3), (9), and (10), the inverse kinematics can be solved directly as

$$\begin{cases} l_i = |\mathbf{R}\mathbf{a}'_i + \mathbf{p} - \mathbf{b}_i| & (i = 1,2,3,4) \\ \phi_{11} = \sin^{-1}(\mathbf{R}(z, -\pi/2) \cdot (\mathbf{R}\mathbf{a}'_1 + \mathbf{p} - \mathbf{b}_1) \cdot (1,0,0)^T) \\ \phi_{21} = \sin^{-1}(\mathbf{R}(z, -\pi) \cdot (\mathbf{R}\mathbf{a}'_2 + \mathbf{p} - \mathbf{b}_2) \cdot (1,0,0)^T) \end{cases} \quad (11)$$

These solutions of the inverse kinematics cover all the configurations and can be used directly corresponding to the topology requirements of the actuation.

**5.2.2 Forward Kinematics.** On the contrary to the inverse displacement analysis, the forward one is to solve the platform position  $\mathbf{p}$  and orientation  $\mathbf{R}$  when giving the corresponding actuation parameters ( $l_i, \phi_{i1}$ ) for each topology. Based on Eq. (9), limb 1 and limb 2 are unified in the kinematics modeling with consideration of two phases. Then, the forward kinematics can be divided into three cases by considering the limb phases of limb 3 and limb 4.

*Case 1: Limb 3 and limb 4 both in phase (rT)<sub>2</sub>PS.* Based on the geometric structure of the platform, there are

$$\begin{cases} (\sqrt{2}r_a)^2 = (\mathbf{a}_1 - \mathbf{a}_2)^2 \\ (2r_a)^2 = (\mathbf{a}_1 - \mathbf{a}_3)^2 \\ 2\sqrt{2}r_a^2 \cos(\pi/4) = (\mathbf{a}_2 - \mathbf{a}_1) \cdot (\mathbf{a}_3 - \mathbf{a}_1) \\ \mathbf{a}_3 \cdot (0,1,0)^T = 0 \\ (\mathbf{a}_1 + \mathbf{a}_3 - \mathbf{a}_2) \cdot (1,0,0)^T = 0 \end{cases} \begin{cases} \phi_{i1} & (\text{rT})_1PS \\ \phi_{i1} = 0 & (\text{rT})_2PS \end{cases} \quad (12)$$

where the first two represent the distances from spherical joint  $A_1$  to  $A_2$  and  $A_3$ , the third one describes the angle  $\angle A_2A_1A_3 = \pi/4$ , the fourth and the fifth are from Eq. (10) for the spherical joint centers of limb 3 and limb 4 constrained on their own planes.

Substituting Eqs. (9) and (10) into Eq. (12) there is

$$\begin{cases} f_1(\phi_{12}, \phi_{22}) = 0 \\ f_2(\phi_{12}, 1, x_3, y_3, z_3, x_3^2, y_3^2, z_3^2) = 0 \\ f_3(\phi_{12}, \phi_{22}, x_3, y_3, z_3) = 0 \\ f_4(y_3) = y_3 = 0 \\ f_5(\phi_{12}, \phi_{22}, x_3, y_3, z_3) = 0 \end{cases} \quad (13)$$

where  $f_i(\bullet)$  is a function of the power products in the bracket.

The last three equations in Eq. (16) are linear functions of  $(x_3, y_3, z_3)$ , thus they can be linearly solved. Substituting the results into  $f_2$  and replacing  $\cos\phi_{i2} = (1 - t_i^2)/(1 + t_i^2)$ ,  $\sin\phi_{i2} = 2t_i/(1 + t_i^2)$  in  $f_1$  and  $f_2$ , there is

$$\begin{cases} f_6(1, t_1^2, t_2^2, t_1 t_2, t_1^2 t_2^2) = 0 \\ f_7(1, t_1^2, t_1^4, t_1^6, t_1^8, t_1^2 t_2^2, \dots, t_1^8 t_2^4) = 0 (j \neq 0) \end{cases} \quad (14)$$

where  $f_6$  and  $f_7$  are linear functions of the power products in the bracket with their coefficients depending on the input parameters only.  $t_i$  is  $\tan(\phi_{i2}/2)$ .

By using Sylvester's dialytic elimination method [40] for the two equations in Eq. (14), a polynomial with only unknown  $t_1$  can be obtained as

$$\sum_{i=0}^{+10} h_{1i} t_1^{2i} = 0 \quad (15)$$

where coefficient  $h_{1i}$  are real constants depending on input data only.

This shows that a univariate equation in  $t_1$  of degree 20 is obtained.

Solving Eq. (15), 20 solutions for  $t_1$  can be obtained. Then,  $t_2$  can be solved by substituting each solution of  $t_1$  back to the equations in Eq. (14) and solving the common roots. Following this,  $(x_3, y_3, z_3)$  can be linearly solved by substituting each pair of solutions of  $t_1, t_2$ , and  $t_3$  into the last three equations in Eq. (13). Based on this, 20 sets of solutions of  $t_1, t_2, t_3$  and  $(x_3, y_3, z_3)$  are obtained and the spherical joint center  $A_i$  can be calculated by substituting  $\phi_{i2} = 2\text{ArcTan}(t_i)$  into Eqs. (9) and (10). Then, the platform position and orientation can be determined using the three spherical joint centers as

$$\begin{cases} \mathbf{u} = (\mathbf{a}_1 - \mathbf{a}_2)/|\mathbf{a}_1 - \mathbf{a}_2| \\ \mathbf{v} = (2\mathbf{a}_3 - \mathbf{a}_1 - \mathbf{a}_2)/|2\mathbf{a}_3 - \mathbf{a}_1 - \mathbf{a}_2| \\ \mathbf{w} = \mathbf{u} \times \mathbf{v}, \mathbf{R} = (\mathbf{u}, \mathbf{v}, \mathbf{w}), \mathbf{p} = \mathbf{a}_1 - r_a \mathbf{u} \end{cases} \quad (16)$$

The real roots correspond to assembly configurations of the 3rTPS parallel mechanism.

*Case 2: One of limb 3 and limb 4 is in phase (rT)<sub>1</sub>PS.* Based on the above analysis, when limb 3 (or limb 4) is in phase (rT)<sub>1</sub>PS, the geometric constraints is the same with Eq. (12) by replacing the fourth (or fifth equation) with  $(\mathbf{a}_3 - \mathbf{b}_3) \cdot (\mathbf{a}_3 - \mathbf{b}_3) = l_3^2$  (or  $(\mathbf{a}_4 - \mathbf{b}_4) \cdot (\mathbf{a}_4 - \mathbf{b}_4) = l_4^2$ ). For both case there is

$$f'_8(1, x_3, y_3, z_3, x_3^2, y_3^2, z_3^2) = 0 \quad (17)$$

It is found that  $f_2$  and  $f'_8$  are linear functions of  $(x_3^2, y_3^2, z_3^2)$  with their coefficients 1. Then a new equation can be obtained from these two by reducing  $(x_3^2, y_3^2, z_3^2)$  as

$$f'_{82}(\phi_{12}, 1, x_3, y_3, z_3) = 0 \quad (18)$$

Thus,  $(x_3, y_3, z_3)$  can be linearly solved from  $f_3, f_5$  in Eq. (13) and  $f'_{82}$  in Eq. (18). Following the same procedure for Eq. (14), there is

$$\begin{cases} f_6(1, t_1^2, t_2^2, t_1 t_2, t_1^2 t_2^2) = 0 \\ f'_7(1, t_1^2, t_1^4, t_1^6, t_1^8, t_1^2 t_2^2, \dots, t_1^8 t_2^4) = 0 (j \neq 0) \end{cases} \quad (19)$$

It can be seen that  $f'_7$  is two order higher than  $f_7$  in terms of  $t_1$ . This is because the order change of the geometric constraints of limb 3 (or limb 4) from 1 with the angle constraint in phase (rT)<sub>2</sub>PS to 2 with limb length constraint in phase (rT)<sub>1</sub>PS.

Similarly, using Sylvester's dialytic elimination method [40] for the two equations in Eq. (19), a polynomial with only unknown  $t_1$  can be obtained as

$$\sum_{i=0}^{+12} h_{2i} t_1^{2i} = 0 \quad (20)$$

where coefficient  $h_{2i}$  are real constants depending on input data only.

This shows a univariate equation in  $t_1$  of degree 24 is obtained which is four order higher than Eq. (15) due to the phase change of limb 3 (or limb 4). The other procedures can follow those in case 1.

*Case 3: Limb 3 and limb 4 are both in phase (rT)<sub>1</sub>PS.* Based on the above analysis, when limb 3 and limb 4 are both in phase (rT)<sub>1</sub>PS, the geometric constraints is the same with Eq. (12) by replacing the fourth and the fifth equations with  $(\mathbf{a}_3 - \mathbf{b}_3) \cdot (\mathbf{a}_3 - \mathbf{b}_3) = l_3^2$  and  $(\mathbf{a}_4 - \mathbf{b}_4) \cdot (\mathbf{a}_4 - \mathbf{b}_4) = l_4^2$ , respectively. There are

$$\begin{cases} f'_4(1, x_3, y_3, z_3, x_3^2, y_3^2, z_3^2) = 0 \\ f'_5(1, x_3, y_3, z_3, x_3^2, y_3^2, z_3^2) = 0 \end{cases} \quad (21)$$

As  $f_2, f'_4$ , and  $f'_5$  are linear functions of  $(x_3^2, y_3^2, z_3^2)$  with their coefficients 1. Then two new equations can be obtained from these two by reducing  $(x_3^2, y_3^2, z_3^2)$  as

$$\begin{cases} f'_{42}(\phi_{12}, 1, x_3, y_3, z_3) = 0 \\ f'_{52}(\phi_{12}, 1, x_3, y_3, z_3) = 0 \end{cases} \quad (22)$$

Thus,  $(x_3, y_3, z_3)$  can be linearly solved from  $f_3$  in Eq. (13) and  $f'_{42}, f'_{52}$  in Eq. (22). Following the same procedure for Eq. (14), there is

$$\begin{cases} f_6(1, t_1^2, t_2^2, t_1 t_2, t_1^2 t_2^2) = 0 \\ f_9(1, t_1^2, t_1^4, t_1^6, t_1^8, t_1^2 t_2^2, \dots, t_1^8 t_2^8) = 0 \quad (j \neq 0) \end{cases} \quad (23)$$

It can be seen that  $f_9$  is two order higher in terms of  $t_1$  and four order higher in terms of  $t_2$  than  $f_7$ . This is because the order change of the geometric constraints of both limb 3 and limb 4 from 1 with the angle constraint in phase  $(rT)_2PS$  to 2 with limb length constraint in phase  $(rT)_1PS$ .

Following Sylvester's dialytic elimination method [40] for the two equations in Eq. (23), a polynomial with only unknown  $t_1$  can be obtained as

$$\sum_{i=0}^{+16} h_{3i} t_1^{2i} = 0 \quad (24)$$

where coefficient  $h_{3i}$  are real constants depending on input data only.

This shows a univariate equation in  $t_1$  of degree 32 is obtained which is 12 order higher than Eq. (15) and eight order higher than Eq. (20) due to the phase change of limb 3 and limb 4. The other procedures can follow those in case 1.

The above procedures solve forward kinematics of all the topologies of the 4rTPS metamorphic parallel mechanism. It can be seen that with the mobility increasing due to topology change, the forward kinematics polynomials has higher order in terms of the unknowns.

## 6 Unified Singularity Modeling With Workspace Analysis

The infinitesimal twist of the moving platform of the 3(rT)PS parallel mechanism can be written as the linear combination of instantaneous twists of each limb

$$\mathbf{S}_G = \dot{\phi}_{i1} \mathbf{S}_{i1} + \dot{\phi}_{i2} \mathbf{S}_{i2} + \dot{l}_i \mathbf{S}_{i3} + \dot{\phi}_{i4} \mathbf{S}_{i4} + \dot{\phi}_{i5} \mathbf{S}_{i5} + \dot{\phi}_{i6} \mathbf{S}_{i6} \quad (i = 1, 2, 3, 4) \quad (25)$$

where  $\mathbf{S}_G$  represents the infinitesimal twist of the moving platform,  $\mathbf{S}_{ij}$  ( $j = 1, 2, 3, 4, 5, 6$ ) denotes the unit screw of the  $j$ th 1-DOF joint in limb  $i$ ,  $\dot{l}_i$  is the distance rate of the prismatic joint in limb  $i$ ,  $\dot{\phi}_{ij}$  ( $j = 1, 2, 4, 5, 6$ ) represent angular rates of the rT joint and spherical joint in limb  $i$ .

Based on the kinematics analysis in Sec. 5, the translation of the prismatic joint is chosen as the input for limb 1 and limb 2 in the phase  $(rT)_2PS$  and the rotation about the radial axis is taken as the second actuation when the limb changes to phase  $(rT)_1PS$ . There is no actuation input from limb 3 and limb 4 when they are in phase  $(rT)_2PS$  and their prismatic joints are actuated in the phase  $(rT)_1PS$ . Thus by locking the active joints in the limbs temporarily and taking the reciprocal product on both sides of Eq. (25), for limb 1 and limb 2 there is

$$[\mathbf{S}'_{i1} \quad \mathbf{S}'_{i2}]^T \circ \mathbf{S}_G = \begin{cases} [0 \quad \dot{l}_i]^T & (rT)_2PS \text{ limb} \\ [\dot{\phi}_{i1} \quad \dot{l}_i]^T & (rT)_1PS \text{ limb} \end{cases} \quad (i = 1, 2) \quad (26)$$

where  $\mathbf{S}'_{i1}$  is the reciprocal screws of geometric constraint to all motion screws in limb  $i$  in phase  $(rT)_2PS$  and it passes through the spherical joint center with the direction parallel to the bracket axis of the rT joint [2].  $\mathbf{S}'_{i1}$  becomes the actuation screw reciprocal to

all the motion screws in Eq. (25) except the actuation joint  $\mathbf{S}_{i1}$  in phase  $(rT)_1PS$  and it passes through the spherical joint center with direction perpendicular to both the limb and the radial axis of the rT joint.  $\mathbf{S}'_{i2}$  is the actuation screw reciprocal to all in Eq. (25) except the prismatic joint screw  $\mathbf{S}_{i3}$  in both limb phases and it is collinear with the limb.

For limb 3 and limb 4 there is

$$\mathbf{S}'_{j1} \circ \mathbf{S}_G = \begin{cases} 0 & (rT)_2PS \text{ limb} \\ \dot{l}_j & (rT)_1PS \text{ limb} \end{cases} \quad (j = 3, 4) \quad (27)$$

where  $\mathbf{S}'_{j1}$  is the reciprocal screws of geometric constraint to all motion screws in limb  $j$  in phase  $(rT)_2PS$  and it has the direction parallel to the bracket axis of the rT joint and passing through the spherical joint center.  $\mathbf{S}'_{j1}$  becomes the actuation screw reciprocal to all the motions screws in Eq. (25) except the actuated prismatic joint  $\mathbf{S}_{i3}$  in phase  $(rT)_1PS$  and with direction collinear with the limb.

Equations in (26) and (27) for the four limbs can be rewritten in matrix form as

$$\begin{bmatrix} \mathbf{S}'_{11} \\ \mathbf{S}'_{12} \\ \mathbf{S}'_{21} \\ \mathbf{S}'_{22} \\ \mathbf{S}'_{31} \\ \mathbf{S}'_{41} \end{bmatrix} \circ \mathbf{S}_G = \mathbf{J} \mathbf{S}_G = \begin{bmatrix} \mathbf{M}_1 \\ \mathbf{b}_1 \times \mathbf{u}_1 & \mathbf{u}_1 \\ \mathbf{M}_2 \\ \mathbf{b}_2 \times \mathbf{u}_2 & \mathbf{u}_2 \\ \mathbf{M}_3 \\ \mathbf{M}_4 \end{bmatrix} \mathbf{S}_G = \begin{bmatrix} g_1 \\ \dot{l}_1 \\ g_2 \\ \dot{l}_2 \\ g_3 \\ g_4 \end{bmatrix} \quad (28)$$

where

$$\text{for } (rT)_2PS : \begin{cases} \mathbf{M}_i = [\mathbf{a}_i \times \mathbf{y} \quad \mathbf{y}], g_i = 0; \\ \mathbf{M}_j = [\mathbf{a}_j \times \mathbf{x} \quad \mathbf{x}], g_j = 0; \\ (i = 1, 3; j = 2, 4) \end{cases}$$

$$\text{for } (rT)_1PS : \begin{cases} \mathbf{M}_i = [\mathbf{a}_i \times (\mathbf{u}_i \times \mathbf{u}_{ir}) \quad \mathbf{u}_i \times \mathbf{u}_{ir}], g_i = \dot{\phi}_{i1}; \\ \mathbf{M}_j = [\mathbf{b}_j \times \mathbf{u}_j \quad \mathbf{u}_j], g_j = \dot{l}_j; \\ (i = 1, 2; j = 3, 4) \end{cases}$$

where  $\mathbf{x} = [1, 0, 0]^T$ ,  $\mathbf{y} = [0, 1, 0]^T$ ,  $\mathbf{u}_i$  is the unit vector of the limb direction, and  $\mathbf{u}_{ir}$  is the unit vector of the radial axis.

Thus,  $\mathbf{J}$  is the 6 by 6 Jacobian matrix. In general, the Jacobian matrix maps the velocities between the manipulator and the actuation input. Once the manipulator meets the singular configuration, this mapping loses its function and the rank of the Jacobian matrix decreases to be less than 6. This can be also interpreted that the six constraint forces in  $\mathbf{J}$  are linearly dependent. Inversely, identifying the dependent conditions for the constraint forces in the workspace will reveal the singular configurations of the manipulator. In order to demonstrate this, some numerical parameters with physical constraints are given as: the platform radius  $r_a = 10$  cm, base radius  $r_b = 20$  cm, spherical joint rotation angle  $\leq \pi/4$  radian, bracket-axis rotation angle  $\phi_{i1} \leq 7\pi/18$  radian, radial axis rotation angle  $\phi_{i2} \leq \pi/2$  radian, limb length  $11 \text{ cm} \leq l_i \leq 22 \text{ cm}$ .

**6.1 Workspace and Singularity Analysis of the 4(rT)<sub>2</sub>PS (2DOF).** The 4(rT)<sub>2</sub>PS parallel mechanism has two bifurcated rotations about  $x$  and  $y$  axes with an independent translation along  $z$ -axis. Based on the given physical parameters above, the workspace of this mechanism is demonstrated in Fig. 5(a), in which the blue parts represent the singularities identified using the Jacobian matrix in Eq. (28) consisting of two actuation forces and four geometric constraint forces. There are three kinds of singular configurations with one that there is no rotation shown in the center in Fig. 5(a). This is the home position in which the platform is parallel to the base and the four geometric constraint forces from the four limbs lie in the same plane as in Fig. 5(b), resulting in one redundant and constraint singularity [26,27] in the home position. Once the platform rotates, it involves into one rotation

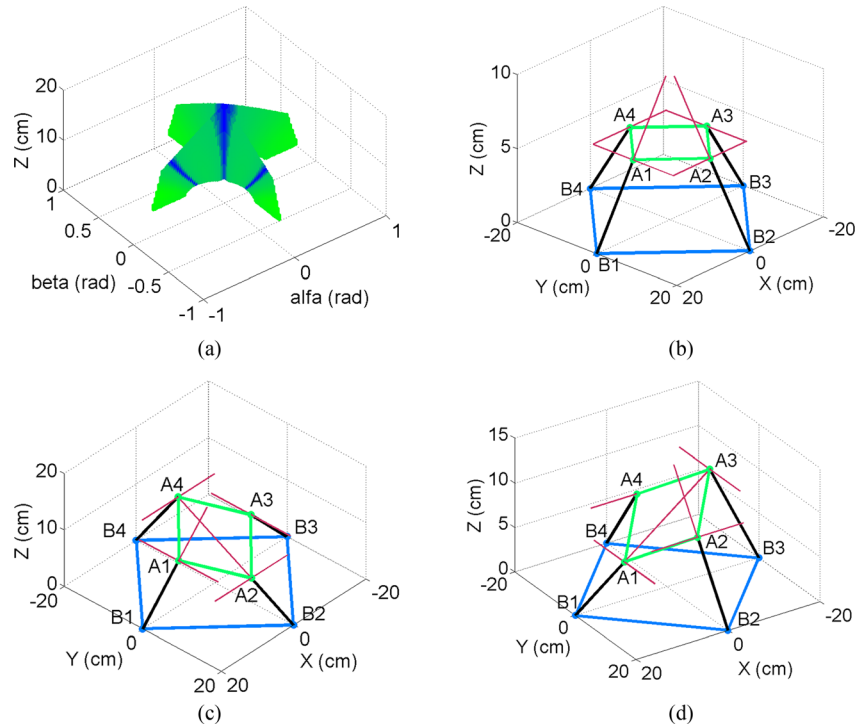


**Fig. 5** Workspace and singular configurations of 4(rT)<sub>2</sub>PS (2DOF) (a) workspace with singularity distribution, (b) singularity 1, (c) singularity 2, and (d) singularity 3

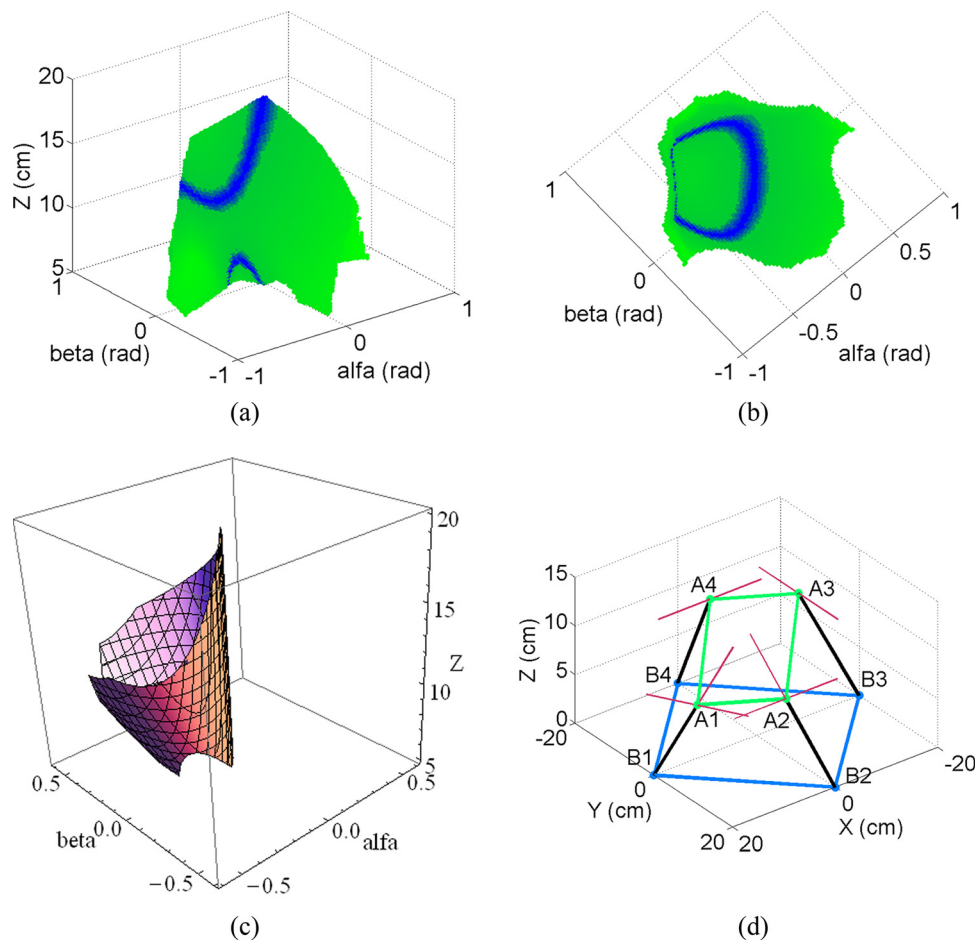
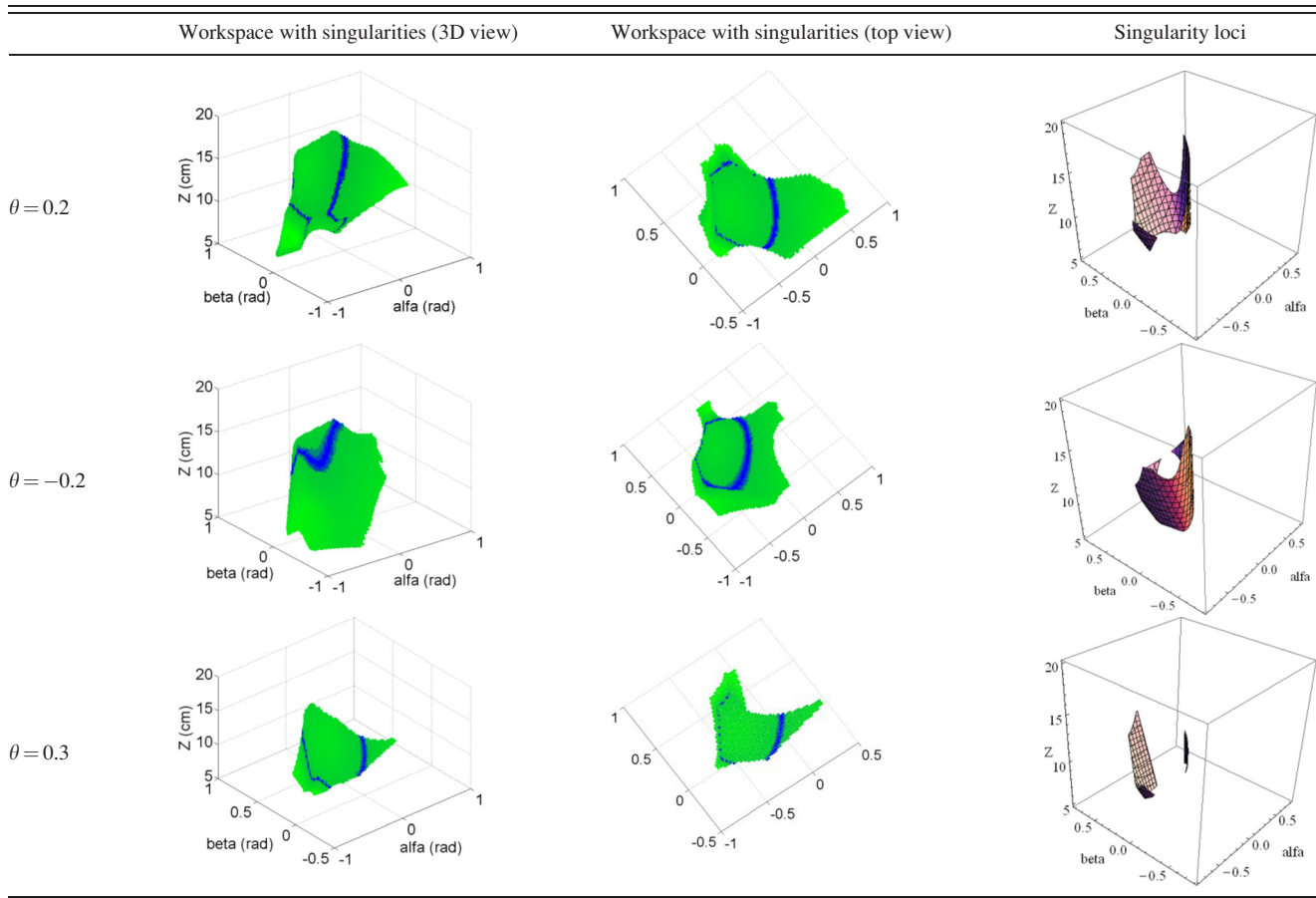


**Fig. 6** Workspace and singularity locus of the 3(rT)<sub>2</sub>PS-1(rT)<sub>1</sub>PS (3DOF) (a) workspace with singularities (3D view), (b) workspace with singularities (top view), (c) singularity locus, (d) singularity 4

**Table 2 Workspace and singularity loci of the  $2(rT)_2PS-2(rT)_1PS$**



branch. As in Fig. 5(c), when the platform rotates about the  $x$ -axis clockwise, a singularity occurs when the actuation force from limb 2 passing through the spherical joint center  $A_4$  in limb 4. In this case, the two geometric constraint forces in limb 2 and limb 4 are parallel to the line  $A_1A_3$  and all the other four constraint forces intersect the line  $A_1A_3$ , resulting in an instantaneous free rotation about the line  $A_1A_3$  with the singular Jacobian of rank five. This is similar when the platform rotates about the  $y$ -axis as shown in Fig. 5(d).

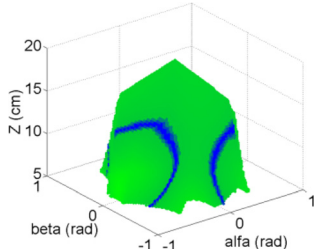
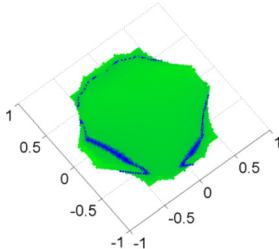
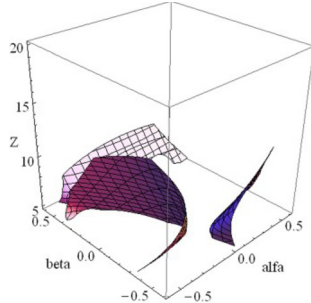
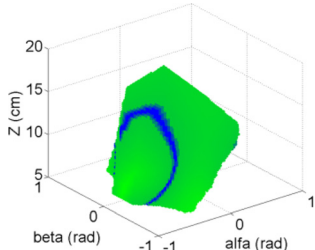
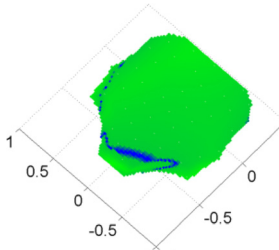
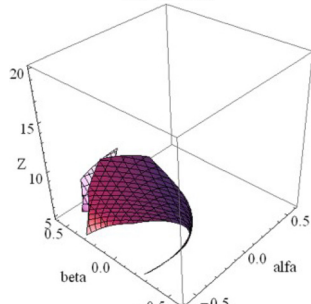
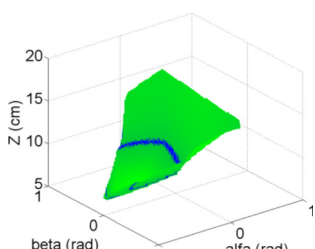
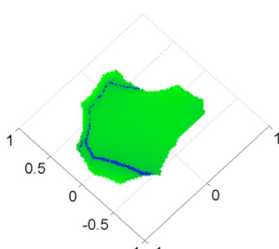
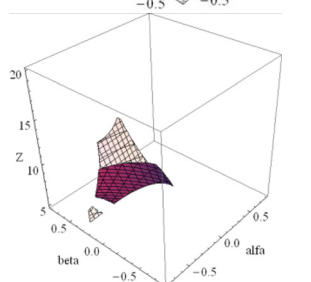
**6.2 Workspace and Singularity Analysis of the  $3(rT)_2PS-1(rT)_1PS$  (3DOF).** When altering the limb 1 from phase 2 to phase 1, the parallel mechanism changes to the  $3(rT)_2PS-1(rT)_1PS$  with two rotational and one translational DOFs. The geometric constraint force in limb 1 becomes the actuation constraint force as in Eq. (28). Based on these, the workspace with singularities are shown in Figs. 6(a) and 6(b) in 3D view and top view, respectively. The singularity points are clearly located in the workspace and a more detailed singularity locus is shown in Fig. 6(c). By investigating the singularity configurations, it can be found that the  $3(rT)_2PS-1(rT)_1PS$  has all the singular configurations of the  $4(rT)_2PS$  in Fig. 5 with one more singular configuration existing as in Fig. 6(d). This singularity is the general complex singularity (Type 5a in Ref. [38]) in which there are six skew constraint forces with one redundant leading to the Jacobian matrix of rank 5.

**6.3 Workspace and Singularity Analysis of the  $2(rT)_2PS-2(rT)_1PS$  (4DOF).** After further changing limb 2 from phase 2 to phase 1, the mechanism becomes the 4DOF  $2(rT)_2PS-2(rT)_1PS$  with three rotational and one translational DOFs. In this case, the six constraint forces in the Jacobian matrix come from two geometric constraint forces in limb 3 and limb 4 with two actuation forces in each of limb 1 and limb 2 as in Eq. (28). By investi-

gating the workspace with different rotations about the  $z$ -axis, singularities in the workspace are shown in Table 2 with the same coordinates in Figs. 5 and 6. When there is no rotation about  $z$ -axis, the workspace with singularities is the same with that in Figs. 6(a) and 6(b). When the platform rotates clockwise or anticlockwise about  $z$ -axis, the workspace becomes smaller with singularity distribution rotates as in Table 2. When rotating the platform about  $z$ -axis from 0.2 to 0.3, the workspace also becomes smaller with less singularity as shown the singularity loci in the third column in Table 2. Comparing with the 3DOF case in Sec. 6.2, all the singular configurations are in the configurations of singularity 1 and singularity 4, while singularity 2 and singularity 3 are avoided when rotating the platform about  $z$ -axis.

**6.4 Workspace and Singularity Analysis of the  $1(rT)_2PS-3(rT)_1PS$  (5DOF).** Based on the 4DOF  $2(rT)_2PS-2(rT)_1PS$  in Sec. 6.3, by altering limb 3 from phase 2 to phase 1, the mechanism becomes the 5DOF  $1(rT)_2PS-3(rT)_1PS$  with three rotational and two translational DOFs. The geometric constraint force parallel to the  $y$ -axis in limb 3 becomes the actuation force along the limb. This eliminates singularity 1 at the home position and singularity 3 as in Fig. 5. The workspace with singularity distribution is shown in Table 3 in terms of different rotations about  $z$ -axis and different translations along  $y$ -axis. Due to the constraint force change in limb 3, the singularity distribution changes a lot while the workspace becomes a little different comparing with the 3DOF  $3(rT)_2PS-1(rT)_1PS$  in Fig. 6. When the platform translates along the  $y$ -axis to the negative side ( $p_y = -3$  in Table 3) without rotating about the  $z$ -axis, the rotational workspace about the  $x$ -axis ( $\alpha$ ) in clockwise becomes smaller, while the singularity keeps similar in the remaining part as shown in Table 3. When there is rotation about  $z$ -axis, the workspace becomes smaller with singularity changes as in Table 3.

**Table 3** Workspace and singularity loci of the  $1(rT)_2PS-3(rT)_1PS$

	Workspace with singularities (3D view)	Workspace with singularities (top view)	Singularity loci
$p_y=0, \theta=0$			
$p_y=-3, \theta=0$			
$p_y=1, \theta=0.2$			

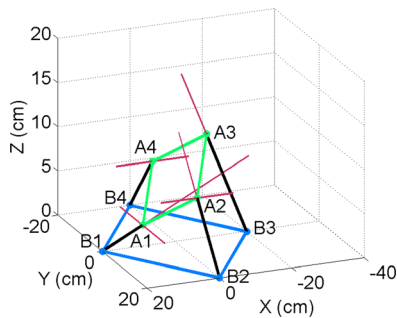


**Fig. 7** Singularity 5

In the workspace of the 5DOF  $1(rT)_2PS-3(rT)_1PS$  parallel mechanism, most singularities occur at the configurations similar to singularity 4 in Fig. 6(d) with six skew constraint forces and some in the configurations similar to singularity 2 in Fig. 6(c). Furthermore, one more singular configuration is found as in Fig. 7 (Type 3b.2 in Ref. [37]). In this case, the plane formed by the parallel constraint forces from limb 2 and limb 4 passes through the intersecting point of the two prismatic-joint-actuation forces in limb 1 and limb 3. One of these four forces is redundant and the Jacobian matrix has rank 5. It occurs when there are anticlockwise pure rotations about the  $y$ -axis.

**6.5 Workspace and Singularity Analysis of the  $4(rT)_1PS$  (6DOF).** After changing all the limb phases from 2 to 1, the mechanism becomes the  $4(rT)_1PS$  parallel mechanism with all the

six DOFs and the six constraint forces in the Jacobian in Eq. (28) are all actuation forces from the four limbs. In order to show and compare the workspace, three samples are listed in Table IV with 3D view workspace and detailed singularity loci. When  $p_x=0$ ,  $p_y=0$ , and  $\theta=0$ , the  $4(rT)_1PS$  has similar workspace with the 5DOF  $1(rT)_2PS-3(rT)_1PS$  in Sec. 6.4 but with much different singularity distribution. Due to the change from geometric constraint parallel to  $x$ -axis to actuation force along the limb in limb 4, the singularities mainly happen when the platform rotates anticlockwise about  $x$ -axis and clockwise about  $y$ -axis as seen from the top-view workspace in the first row in Table 4. By investigating the singularities, it is found that most singular configurations come from the singularity 4 case in Fig. 6(d) with six skew forces and one redundant. Another singular configuration has all the six constraint forces intersecting the  $A_1A_2$  line, which is similar to singularity 2 and singularity 3 in Fig. 5 and the platform has an instantaneous rotation about the  $A_1A_2$  line. One more case as singularity 6 in Fig. 8(a) is found at the home position when the platform is parallel to the base with only translation along  $z$ -axis and the four actuation forces along the four limbs intersecting at one point, resulting one redundant.

When setting  $p_x=0$ ,  $p_y=0$ , and  $p_z=10$ , the workspace with three rotations and singularity distribution is shown in the second row in Table 4. Similarly, the singularities mainly locate at the side when the platform rotates anticlockwise about  $x$ -axis and clockwise about  $y$ -axis. Singular configurations are also similar with the first case in Table 4.

When setting all the rotations zero, the platform will experience pure translations. However, the four actuation forces along the four limbs always intersect at one point in this case as singularity

**Table 4 Workspace and singularity loci of the 4(rT)<sub>1</sub>PS**

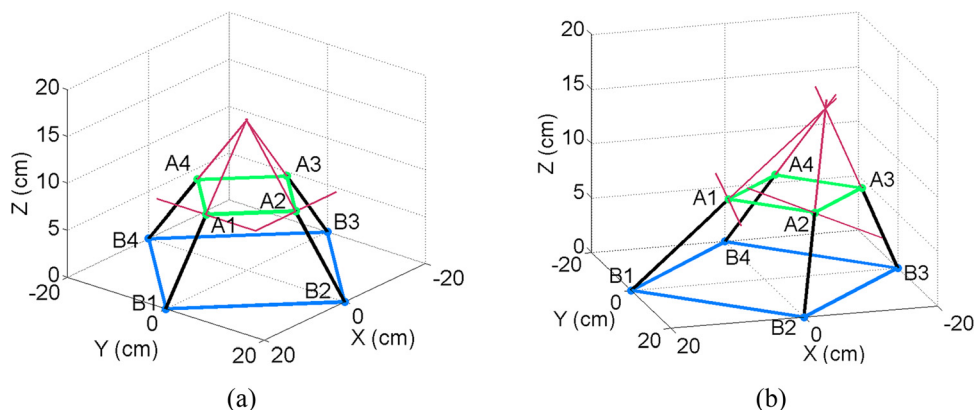
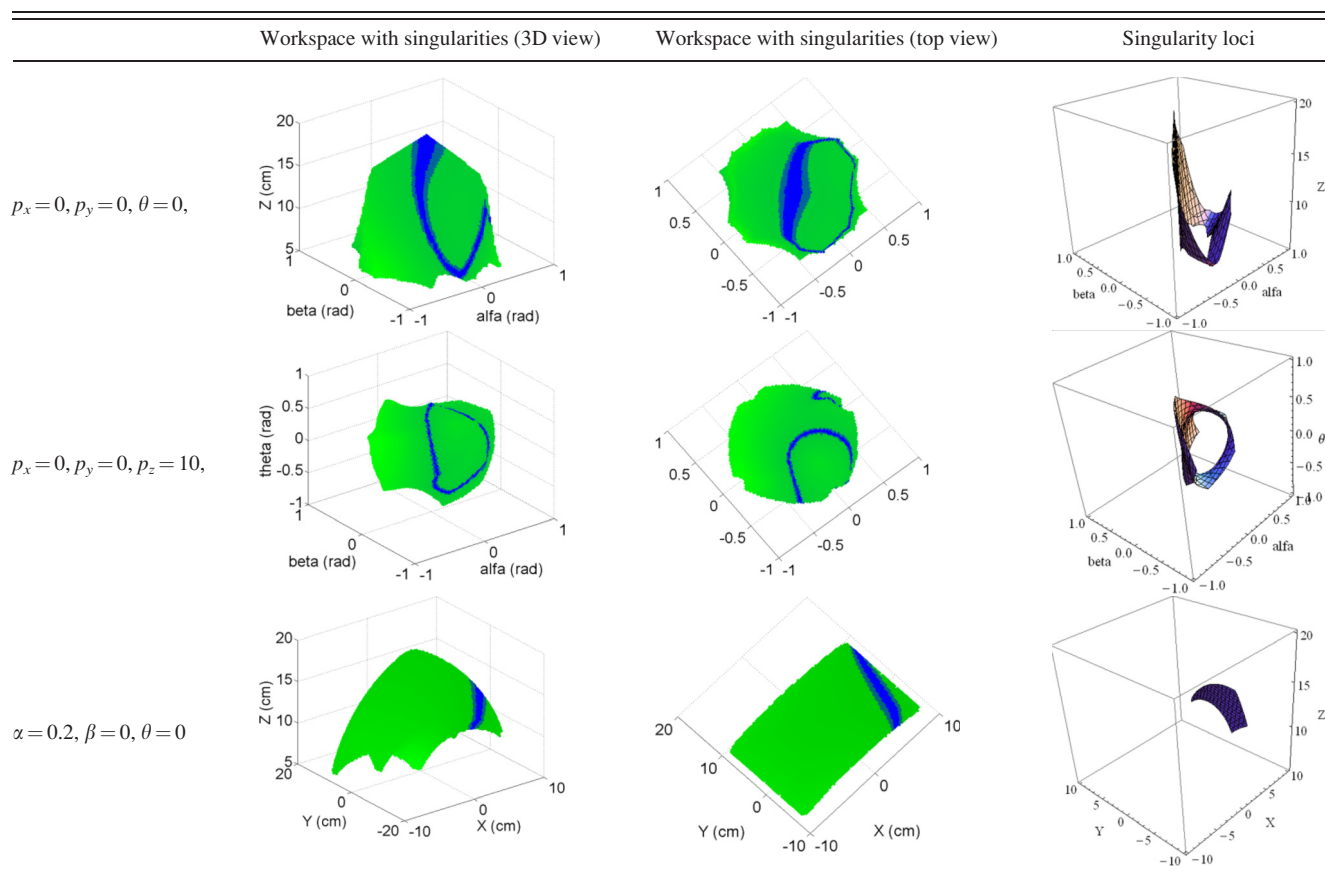


**Fig. 8 Singularity 6 in two different configurations (a) home position (b) a general configuration ( $p_x = -4, p_y = 2,$  and  $p_z = 8$ )**

6 in Fig. 8(b). After rotating the platform about z-axis, the configurations are still under singularity due to the fact that the four forces lie on the same regulus [38] with one redundant. The rotation about x or y axes can help avoid this singular problem as shown in the third row in Table 4 with a rotation ( $\alpha=0.2$ ) about x-axis. Most part of the workspace is singularity free while some singularities exist when the platform translates to the positive side of x-axis which causes singularity with six skew forces. The situation is similar when the platform rotates about y-axis.

The workspace and singularity analysis shows all the singularities in the workspace which can be used to reduce singularities in the design of the 4rTPS mechanism and free-singularity workspace can be used in the application motion plan. Take the 2-DOF bifurcated motion for example, singularities are found when the

platform is parallel to the base and when the platform rotates to the positive sides of x-axis and y-axis as shown in Fig. 5(a). One more actuator can be used to solve the constraint singularity when the platform is parallel to the base, while the motion plan can focus on the negative sides of x-axis and y-axis to avoid all the singularities. This is the same for all the other topologies as shown in Fig. 6 and Tables 2–4. Thus, these singularities of the 4rTPS mechanism can be avoided in the applications.

## 7 Conclusions

This paper presented reconfiguration, kinematics and singularity analysis of a new metamorphic parallel mechanism consisting of four reconfigurable rTPS limbs. Stemming from the

configuration change of the reconfigurable Hooke (rT) joint, the rTPS limb has two phases while in one phase it has mobility six and in the other it provides a geometric constraint to the platform by constraining the spherical joint center lie on a plane. It was found that the platform had bifurcated rotation in two perpendicular directions with a common translation in the topology with mobility 2. By changing the limb phases with different numbers and orders of the four limbs, the mechanism demonstrated various topologies with mobility change from 2 to 6 in different types. Considering the difference between the limb phases, a unified kinematics modeling of the rTPS limb was proposed by taking one phase as a special case of the other. Based on this, both inverse and forward kinematics modeling for all topologies of the mechanism was obtained and solved analytically by combining different limb phase models. It was found that the forward kinematics has 20, 24, or 32 solutions due to the order change of the limb constraint equations from angle constraint to length constraint. By including the geometric constraint forces and actuation forces in the Jacobian matrix, unified singularity analysis was demonstrated with singularity loci shown in the workspace. With the constraint force change in the reconfigured topologies, singularity configurations were found different due to the geometric conditions. Singularity-free workspace was clearly illustrated in each mechanism topology with mobility from 2 to 6.

## References

- [1] Merlet, J. P., 2008, *Parallel Robots*, 2nd ed., Springer, New York.
- [2] Gan, D. M., Dai, J. S., and Liao, Q. Z., 2009, "Mobility Change in Two Types of Metamorphic Parallel Mechanisms," *ASME J. Mech. Rob.*, **1**, p. 041007.
- [3] Dai, J. S., and Rees, J. J., 1999, "Mobility in Metamorphic Mechanisms of Foldable/Erectable Kinds," *ASME J. Mech. Des.*, **121**(3), pp. 375–382.
- [4] Wohlhart, K., 1996, "Kinematotropic Linkages," *Advances in Robot Kinematics*, J. Lenarcic and V. Parenti-Castelli, eds., Kluwer, Dordrecht, pp. 359–368.
- [5] Parise, J. J., Howell, L. L., and Magleby, S. P., 2000, "Ortho-Planar Mechanisms," Proceedings of 26th Biennial Mechanisms and Robotics Conference, Baltimore, MD, Sept., Paper No. DETC2000/MECH-14193.
- [6] Chen, I. M., Li, S. H., and Cathala, A., 2003, "Mechatronic Design and Locomotion of Amoebot—A Metamorphic Underwater Vehicle," *J. Rob. Syst.*, **20**(6), pp. 307–314.
- [7] Liu, C., and Yang, T., 2004, "Essence and Characteristics of Metamorphic Mechanisms and Their Metamorphic Ways," Proceedings of 11th World Congress in Mechanism and Machine Science, Tianjing, China, April, pp. 1285–1288.
- [8] Dai, J. S., and Rees, J. J., 2005, "Matrix Representation of Topological Changes in Metamorphic Mechanisms," *ASME J. Mech. Des.*, **127**(4), pp. 837–840.
- [9] Yan, H. S., and Kuo, C. H., 2006, "Topological Representations and Characteristics of Variable Kinematic Joints," *ASME J. Mech. Des.*, **128**(2), pp. 384–391.
- [10] Kuo, C. H., and Yan, H. S., 2007, "On the Mobility and Configuration Singularity of Mechanisms With Variable Topologies," *ASME J. Mech. Des.*, **129**, pp. 617–624.
- [11] Fanghella, P., Galletti, C., and Giannotti, E., 2006, "Parallel Robots that Change Their Group of Motion," *Advances in Robot Kinematics*, Springer, New York, pp. 49–56.
- [12] Xi, F., Xu, Y., and Xiong, G., 2006, "Design and Analysis of a Re-Configurable Parallel Robot," *Mech. Mach. Theory*, **41**, pp. 191–211.
- [13] Kong, X., Gosselin, C. M., and Richard, P. L., 2007, "Type Synthesis of Parallel Mechanisms With Multiple Operation Modes," *ASME J. Mech. Des.*, **129**(7), pp. 595–601.
- [14] Dai, J. S., and Wang, D., 2007, "Geometric Analysis and Synthesis of the Metamorphic Robotic Hand," *ASME J. Mech. Des.*, **129**(11), pp. 1191–1197.
- [15] Zhang, L. P., Wang, D. L., and Dai, J. S., 2008, "Biological Modeling and Evolution Based Synthesis of Metamorphic Mechanisms," *ASME J. Mech. Des.*, **130**, p. 072303.
- [16] Zhang, K. T., Dai, J. S., and Fang, Y. F., 2010, "Topology and Constraint Analysis of Phase Change in the Metamorphic Chain and Its Evolved Mechanism," *ASME J. Mech. Des.*, **132**(12), p. 121001.
- [17] Gan, D. M., Dai, J. S., and Liao, Q. Z., 2010, "Constraint Analysis on Mobility Change of a Novel Metamorphic Parallel Mechanism," *Mech. Mach. Theory*, **45**(12), pp. 1864–1876.
- [18] Gan, D. M., Dai, J. S., and Caldwell, D. G., 2011, "Constraint-Based Limb Synthesis and Mobility-Change Aimed Mechanism Construction," *ASME J. Mech. Des.*, **133**(5), 051001.
- [19] Wampler, C. W., 2006, "On a Rigid Body Subject to Point-Plane Constraints," *ASME J. Mech. Des.*, **128**(1), pp. 151–158.
- [20] Selig, J. M., 2011, "On the Geometry of Point-Plane Constraints on Rigid-Body Displacements," *Acta Appl. Math.*, **116**(2), pp. 133–155.
- [21] Karouia, M., and Hervé, J. M., 2002, "A Family of Novel Orientational 3-DOF Parallel Robots," Proceedings of 14th CISM-IFTOMM RoManSy, Springer, pp. 359–368.
- [22] Lee, C. C., and Hervé, J. M., 2009, "Uncoupled 6-DOF Tripods Via Group Theory," Proceedings of the 5th International Workshop on Computational Kinematics, A. Kecskeméthy and A. Müller, eds. Springer, pp. 201–208.
- [23] Li, Q., and Hervé, J. M., 2010, "1T2R Parallel Mechanisms Without Parasitic Motion," *IEEE Trans. Rob. Autom.*, **26**(3), pp. 401–410.
- [24] Li, Q., and Hervé, J. M., 2009, "Parallel Mechanisms With Bifurcation of Schoenflies Motion," *IEEE Trans. Rob. Autom.*, **25**(1), pp. 158–164.
- [25] Gogu, G., 2011, "Maximally Regular T2R1-Type Parallel Manipulators With Bifurcated Spatial Motion," *ASME J. Mech. Rob.*, **3**(1), p. 011010.
- [26] Zlatanov, D., Bonev, I. A., and Gosselin, C. M., 2002, "Constraint Singularities of Parallel Mechanisms," Proceedings of IEEE International Conference on Robotics and Automation, Washington, D.C., pp. 496–502.
- [27] Zlatanov, D., Bonev, I. A., and Gosselin, C. M., 2002, "Constraint Singularities as C-Space Singularities," *Advances in Robot Kinematics*, J. Lenarcic and F. Thomas, eds., Kluwer, Dordrecht, pp. 183–192.
- [28] Jeong, Y. K., Lee, D. J., Kim, K. H., and Park, J. O., 2000, "A Wearable Robotic Arm With High Force-Reflection Capability," Proceedings of the 2000 IEEE International Workshop on Robot and Human Interactive Communication, Sept. 27–29, Osaka, Japan, pp. 411–416.
- [29] Grosch, P., Di Gregorio, R., López, J., and Thomas, F., 2010, "Motion Planning for a Novel Reconfigurable Parallel Manipulator With Lockable Revolute Joints," Proceedings of the 2010 IEEE International Conference on Robotics and Automation, Anchorage, Alaska, May 3–8.
- [30] Liao, Q. Z., Seneviratne, L. D., and Earles, S. W. E., 1995, "Forward Positional Analysis for the General 4–6 In-Parallel Platform," *Proc. Inst. Mech. Eng., Part C: Mech. Eng. Sci.*, **209**(1), pp. 55–67.
- [31] Gan, D. M., Liao, Q. Z., Dai, J. S., Wei, S. M., and Seneviratne, L. D., 2009, "Forward Displacement Analysis of the General 6–6 Stewart Mechanism Using Grobner Bases," *Mech. Mach. Theory*, **44**(9), pp. 1640–1647.
- [32] Gosselin, C., and Angeles, J., 1990, "Singularity Analysis of Closed-Loop Kinematic Chains," *IEEE Trans. Rob. Autom.*, **6**(3), pp. 281–290.
- [33] Zlatanov, D., Fenton, R. G., and Benhabib, B., 1995, "A Unifying Framework for Classification and Interpretation of Mechanism Singularities," *ASME J. Mech. Des.*, **117**, pp. 566–572.
- [34] Merlet, J. P., 2007, "A Formal-Numerical Approach for Robust In-Workspace Singularity Detection," *IEEE Trans. Rob. Autom.*, **23**(3), pp. 393–402.
- [35] Kong, X., and Gosselin, C., 2001, "Uncertainty Singularity Analysis of Parallel Manipulators Based on the Instability Analysis of Structures," *Int. J. Robot. Res.*, **20**(11), pp. 847–856.
- [36] Tsai, L. W., 1998, "The Jacobian Analysis of a Parallel Manipulator Using Reciprocal Screws," *Adv. Robot Kinematics*, J. Lenarčič, M. L. Husty, eds., Kluwer, Dordrecht, pp. 327–336.
- [37] Hao, F., and McCarthy, J. M., 1998, "Conditions for Line-Based Singularities in Spatial Platform Manipulators," *J. Rob. Syst.*, **15**(1), pp. 43–55.
- [38] Merlet, J. P., 1989, "Singular Configurations of Parallel Manipulators and Grassmann Geometry," *Int. J. Robot. Res.*, **8**(5), pp. 45–56.
- [39] Ben-Horin, P., and Shoham, M., 2006, "Singularity Condition of Six-Degree-of-Freedom Three-Legged Parallel Robots Based on Grassmann–Cayley Algebra," *IEEE Tran. Robotics*, **22**(4), pp. 577–590.
- [40] Bottema, O., and Roth, B., 1979, *Theoretical Kinematics*, North-Holland, New York.